IEEE Access
Multidisciplinary | Rapid Review | Open Access Journal

Received 15 October 2023, accepted 21 October 2023, date of publication 25 October 2023, date of current version 1 November 2023.

Digital Object Identifier 10.1109/ACCESS.2023.3327425

RESEARCH ARTICLE

A Robust Sliding Mode and PI-Based Tracking Control for the MIMO "DC/DC Buck Converter–Inverter–DC Motor" System

ROGELIO ERNESTO GARCÍA-CHÁVEZ[1], RAMÓN SILVA-ORTIGOZA[1], (Member, IEEE), VICTOR MANUEL HERNÁNDEZ-GUZMÁN[2], (Member, IEEE), MAGDALENA MARCIANO-MELCHOR[1], ÁNGEL ADRIÁN ORTA-QUINTANA[1], JOSÉ RAFAEL GARCÍA-SÁNCHEZ[3], AND HIND TAUD[1], (Member, IEEE)

[1]Laboratorio de Mecatrónica y Energía Renovable, CIDETEC, Instituto Politécnico Nacional, Ciudad de México 07700, Mexico
[2]Facultad de Ingeniería, Centro Universitario, Universidad Autónoma de Querétaro, Querétaro 76010, Mexico
[3]División de Ingeniería Mecatrónica, Tecnológico de Estudios Superiores de Huixquilucan, Tecnológico Nacional de México, Estado de México 52773, Mexico

Corresponding authors: Ramón Silva-Ortigoza (rsilvao@ipn.mx) and Victor Manuel Hernández-Guzmán (vmhg@uaq.mx)

This work was supported by Instituto Politécnico Nacional (IPN), Mexico. The work of Rogelio Ernesto García-Chávez and Ángel Adrián Orta-Quintana was supported by CONAHCYT-México and BEIFI Scholarships. The work of Ramón Silva-Ortigoza, Magdalena Marciano-Melchor, and Hind Taud was supported in part by SNII-CONAHCYT-México, and in part by IPN Programs EDI and SIBE. The work of Victor Manuel Hernández-Guzmán and José Rafael García-Sánchez was supported by SNII-CONAHCYT-México.

ABSTRACT This work addresses the control problem related to the bidirectional velocity of a DC motor fed by a DC/DC Buck converter–inverter as power amplifier. While various power electronic topologies have been proposed in the literature, this research focuses on one that was previously disregarded due to its delivery of pulse width modulated voltage signals instead of smooth voltage signals to the DC motor. However, in this paper it is demonstrated that by appropriately controlling the power electronic converter it is indeed possible to deliver the desired smooth voltage signals to the motor. Moreover, the proposed control strategy is robust, employing multiple proportional-integral loops, and a sliding mode controller. A formal proof of asymptotic stability is provided and the robustness is verified through experimental validation.

INDEX TERMS Power electronic converter, DC motor, bidirectional velocity control, proportional-integral control, sliding mode control.

I. INTRODUCTION

PWM, or pulse width modulation, is currently the prevailing method employed for providing power to closed-loop controlled electromechanical systems. This technique allows to provide power just by switching power transistors and it tries to exploit the fact that the power dissipated by the transistor is very small because it ideally operates only at saturation (maximal current and zero voltage) or at cut-off (maximal voltage and zero current). Nevertheless, the process of switching transistors in a hard manner places significant strain on the electrical subsystem of the plant due to the sudden fluctuations related to electric currents and voltages [1].

To address the aforementioned issue, DC/DC power electronic converters as power amplifiers has been suggested [2]. These converters have the capability to generate voltages and electric currents smooth enough due to the presence of capacitors and inductors within their design. By employing these converters, the noise commonly generated by the abrupt switching in PWM-based power amplifiers is reduced.

The above ideas have inspired numerous studies on the control of DC motors when operated using different DC/DC power electronic converters topologies. Among these, the Buck [3], [4], [5], [6], [7], [8], [9], [10], [11], [12], [13], [14], [15], [16], [17], [18], [19], [20], [21], [22], [23], the Boost [24], [25], [26], [27], [28], [29], [30], and the Buck-Boost

The associate editor coordinating the review of this manuscript and approving it for publication was Jiann-Jong Chen.

© 2023 The Authors. This work is licensed under a Creative Commons Attribution 4.0 License.
For more information, see https://creativecommons.org/licenses/by/4.0/

[31], [32] topologies have emerged as the most commonly utilized ones. Other topologies of DC/DC power converters used in the control of DC motors include the following: [33] for the Ćuk converter and [28], [34] for the Luo converter. However, the previously mentioned works only consider velocity control in one sense of rotation. This limitation arises because of the intrinsic incapability of the utilized DC/DC power electronic converter topologies to generate bipolar voltage.

This constraint prompted further investigation, wherein a full H bridge inverter was introduced connecting the DC/DC power electronic converter and the DC motor. Thus, for these new connections, the topology utilizing a DC/DC Buck converter was studied in [35], [36], [37], and [38]. Similarly, the configuration involving a DC/DC Boost converter was presented in [39], [40], and [41]. Furthermore, in [42], [43], [44], and [45], the connection employing a DC/DC Buck-Boost converter was utilized. And, in [46] the DC/DC Sepic converter–inverter–DC motor system was exposed. Although it was demonstrated theoretically and experimentally that bipolar voltage can be delivered to DC motor, the main drawback in [35], [39], [42], and [46] is that this voltage is, however, still a PWM signal. As a result of this drawback, research was redirected towards a different power converter topology where the DC/DC part of the power converter is placed between the full H bridge inverter and DC motor (see the series of works [47], [48], [49]). This topology has been so successful that it has been applied to control permanent magnet syncnronous motors (PMSM) [50], induction motors (IM) [51], and DC motor-actuated wheeled mobile robots (WMR) [52]. Lastly, alongside the state-of-the-art in DC motors driven by DC/DC converters, interesting papers have recently been published addressing the control of DC/DC converters and the control of DC motors as separate problems. In this direction, on the one hand, contributions related to the Buck converter have been analyzed in [53], [54], and [55], while new control schemes for the Boost and Buck-Boost topologies were presented in [56], [57], [58], [59], [60], and [61], respectively. On the other hand, regarding DC motor control new designs have recently been introduced in [62], [63], [64], and [65].

In the present paper, the converter topology introduced in [35] is considered. Theoretical and experimental analyses reveal that the proposed topology in [35] enables the delivery of smooth voltage and electric current signals, as opposed to their pulse width modulation (PWM) counterparts. This capability is achieved through effective control strategies implemented in the topology. The control strategy presented in this study, designed to address the aforementioned issue, consists of multiple proportional-integral (PI) loops and a sliding mode loop specifically designed to regulate the electric current passing through the converter inductor. As demonstrated through experimental validation, this approach yields a robust control scheme that effectively handles both uncertainties in plant parameters and external disturbances. Although this research only prove asymptotic stability at local level of the equilibrium of interest, the merit of this result is simplicity of the developed control scheme despite the complexity of the plant. In this respect, it is well known in the control community that the control problem complicates in nonlinear systems when considering additional electrical dynamics (i.e., the electronic power converter) between controller and DC motor. Moreover, stability proof of simple PI loops is also complicated in nonlinear electromechanical control systems. See [66] for a recent solution to such a control problem. As will be shown in the next section, plant under study in the present paper is nonlinear because of inverter. The aforementioned features outlined in this paragraph constitute the primary contributions of this study.

Finally, a few comments regarding notation. Let $h \in \mathcal{R}^n$ be a vector, where $\|h\|_1 = \sum_{i=1}^{n} |h_i|$ is the 1-norm, and $|\cdot|$ is the absolute value function. Also, $\|h\| = \sqrt{\sum_{i=1}^{n} h_i^2}$ corresponds to the Euclidean norm. Given a symmetric matrix A of $n \times n$, all of its eigenvalues are real and $\lambda_{min}(A)$ stands for its minimum eigenvalue.

II. DYNAMIC MODEL

Fig. 1 depicts the MIMO "DC/DC Buck converter–inverter–DC motor" system. The following dynamic behavior was found in [35] by applying Kirchhoff's Laws to Fig. 1 when modeling transistors and diode by means of ideal switches:

$$L\frac{di}{dt} = -\upsilon + Eu_1, \tag{1}$$

$$C\frac{d\upsilon}{dt} = i - i_a u_2 - \frac{\upsilon}{R}, \tag{2}$$

$$L_a\frac{di_a}{dt} = \upsilon u_2 - R_a i_a - k_e\omega, \tag{3}$$

$$J\frac{d\omega}{dt} = k_m i_a - B\omega - T_L. \tag{4}$$

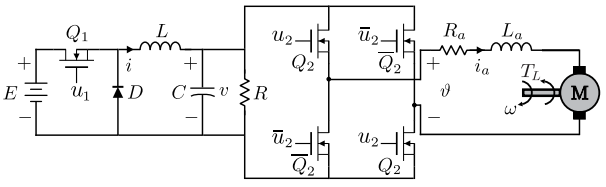

FIGURE 1. Electric diagram of the MIMO "DC/DC Buck converter–inverter–DC motor" system.

Variable i is the electric current passing through the inductance L of the converter, while υ is the voltage across the output capacitance C of the converter (this is, the voltage provided to the input terminals of the inverter). The output terminals of the inverter are connected to the DC motor's terminals. The voltage at the DC motor terminals is denoted as $\vartheta = \upsilon u_2$. The electric current passing through the DC motor armature and the velocity of the motor shaft are denoted as i_a and ω, respectively. Variables u_1 and u_2 are the two system inputs and represent the positions of switches that model transistor Q_1, diode and transistors Q_2, respectively. Variable $\bar{u}_2$, that models transistors $\bar{Q}_2$, is the complement of

u_2. Variable u_1 only takes the discrete values 0 or 1, whereas variable u_2 only takes the discrete values -1 or 1. See [35] for further details. Notice that mathematical model in (1)–(4) is nonlinear because of products $i_a u_2$ and υu_2.

The constants E, R, R_a, L_a, k_e, k_m, J, and B, are all positive and represent the power supply voltage, a fixed resistance at the output of the converter, the resistance and the inductance, both of the armature, the motor back electromotive force, the motor torque, motor inertia, and the viscous friction coefficient, respectively. Additionally, T_L represents an unvarying and unidentified load torque applied to the motor shaft.

The following saturation function is considered.

Definition 2.1: Consider the following odd saturation function (see Fig. 2(a)):

$$zat(x) = \begin{cases} \dfrac{M}{\beta_0}x, & |x| < \beta_0 - \mu \\ M - k|(x-(\beta_0+\mu))^{p_0}|, & \beta_0-\mu \le x < \beta_0+\mu \\ -(M-k|(x+\beta_0+\mu)^{p_0}|), & -(\beta_0+\mu) < x \le -(\beta_0-\mu) \\ M, & x \ge \beta_0+\mu \\ -M, & x \le -(\beta_0+\mu), \end{cases} \tag{5}$$

where $\beta_0 = \alpha_1 M$, $\mu = \alpha_0\beta_0$ and $0 < \alpha_0 < 1$, $0 < \alpha_1 < 1$ are constants. Function $zat(x)$ is continuously differentiable such that:

$$0 \le \frac{dzat(x)}{dx} \le \frac{M}{\beta_0}, \quad \forall x \in \mathcal{R}, \tag{6}$$

if:

$$p_0 = \frac{2M\mu}{\beta_0}\frac{1}{M - \frac{M}{\beta_0}(\beta_0 - \mu)}, \tag{7}$$

$$k = \frac{M}{\beta_0 p_0}\frac{1}{(2\mu)^{p_0-1}}. \tag{8}$$

Fig. 2(b) presents a family of plots for $zat(x)$ using M constant, a constant $0 < \alpha_0 < 1$ and different values for $0 < \alpha_1 < 1$. It is clear that $zat(x) \to sign(x)$, if $M = 1$, as $\alpha_1 \to 0$, i.e., as $\beta_0 \to 0$, where:

$$sign(x) = \begin{cases} +1, & x \ge 0 \\ -1, & x < 0. \end{cases} \tag{9}$$

Finally, let us point out that saturation function defined in (5) have some advantages over other saturation functions such as sigmoid or tanh functions. These advantages are that (5) i) represents a better approximation to sign function, ii) is linear in $[-(\beta_0 - \mu), \beta_0 - \mu]$, and iii) its derivative is constant and equal to M/β_0 in $[-(\beta_0 - \mu), \beta_0 - \mu]$.

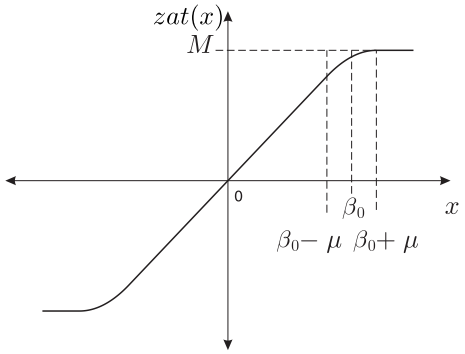

(a) $zat(x)$ is a continuously differentiable odd function.

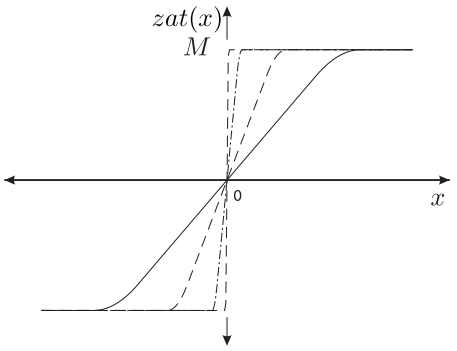

(b) M, α_0, are constant. Continuous: $\alpha_1 = 0.9$, Steep-dashed: $\alpha_1 = 0.01$.

FIGURE 2. The saturation function *zat*(*x*) introduced in Definition 2.1.

III. CONTROL OF THE MIMO "DC/DC-BUCK CONVERTER–INVERTER–DC MOTOR" SYSTEM

The main result is outlined in the following proposition.

Proposition 3.1: Consider the dynamics of the MIMO "DC/DC Buck converter–inverter–DC motor" system (1)-(4) with the following controller in closed-loop:

$$u_1 = \frac{1}{2}[1 - sign(s)], \quad s = i - i^*, \tag{10}$$

$$i^* = \frac{\overline{\upsilon}}{R}zat(\overline{\upsilon}) + k_{p1}e + k_{i1}\int_0^t e(\tau)d\tau, \tag{11}$$

$$\overline{\upsilon} = -r_a e_a + R_a\bar{i}_a - \gamma\int_0^t e_a(\tau)d\tau + fk_{p2}\tilde{\omega}, \tag{12}$$

$$\bar{i}_a = k_{i2}\int_0^t \tilde{\omega}(\tau)d\tau, \quad e = \overline{\upsilon}zat(\overline{\upsilon}) - \upsilon, \tag{13}$$

$$e_a = i_a - \bar{i}_a, \quad \tilde{\omega} = \omega_d - \omega, \quad u_2 = zat(\overline{\upsilon}), \tag{14}$$

where functions $sign(s)$ and $zat(\overline{\upsilon})$ are defined in (9) and Definition 2.1, for $M = 1$, respectively. The desired velocity, denoted as $\omega_d(t)$, is a rest-to-rest time-varying function such that $\dot{\omega}_d(t)$ is bounded. Moreover, $\omega_d(t_i) = \omega_{di}$ at some $t = t_i \ge 0$ for some constant ω_{di} and $\omega_d(t) = \overline{\omega}_d$ for some finite t_f such that $t \ge t_f > t_i$ and $\overline{\omega}_d$ is another finite constant. We assume that $|\omega_d| > 0$ for all $t \ge 0$, excepting, perhaps, some isolated points of time.

To achieve asymptotic stability within the closed-loop system, values $k_{p1}, k_{i1}, k_{p2}, k_{i2}, f, r_a$, and γ greater than zero must exist and need to satisfy the following condition:

$$0 < \upsilon(t) + L\frac{di^*(t)}{dt} < E. \tag{15}$$

Remark 3.1: According to Section II, u_2 represents commutation of transistors Q_2 and such a commutation is ideally modeled as a discontinuous sign function. Hence, u_2 is restricted to assume exclusively discrete values -1 and $+1$. On the other hand, in real power electronic devices the actual commutation represented by variable u_2 is likely to behave as the function $zat(\bar{v})$ when $M = 1$ and $\beta_0 \to 0$, i.e., when $\alpha_1 \to 0$ in Fig. 2(b).

Thus, the intention to define $u_2 = zat(\overline{v})$, in Proposition 3.1, as a continuously differentiable function is fourfold: *a*) it accurately represents a variable taking only two discrete values -1 and $+1$, *b*) it accurately represents the actual commutation that is present in practical power electronic devices, *c*) the derivative of u_2 is well defined and this allows the mathematical procedure presented below in the proof of Proposition 3.1, and *d*) for practical purposes, i.e., in experiments, $u_2 = sign(\overline{v})$ can be implemented as a variable taking only the discrete values -1 and $+1$ using the $sign(\cdot)$ function defined in (9).

Remark 3.2: The controller in Proposition 3.1, i.e., (10)-(14), contains four main loops. See, for instance, block "Bidirectional tracking robust control" in Fig. 3. *a*) There is a sliding modes controller in the most internal loop, which aims to regulate the electric current i to achieve the desired profile i^* of the electric current passing through the converter inductor. *b*) A linear proportional-integral (PI) controller computes the desired electric current i^* based on the error between the converter output voltage v and its desired profile $\bar{v}$. *c*) Another linear PI controller, augmented with terms involving velocity error and its integral, generates the desired converter output voltage $\bar{v}$ based on the error related to the motor's armature electric current. *d*) The desired electric current $\bar{i}_a$, associated with motor's armature, is derived by integrating the velocity error. This control strategy incorporates proportional and integral actions, fundamental components commonly used in industrial DC motor control, on 1) the armature electric current error and 2) velocity error. The utilization of sliding modes control for managing the electric current passing through the converter inductor, along with the integration of proportional and integral actions to address the converter output voltage error, enhances the anticipated robustness of the closed-loop system. The experimental verification of robustness is presented in Section IV.

A. REACHING THE SLIDING SURFACE

Considering the positive definite scalar and radially unbounded function $V(s) = \frac{1}{2}s^2$ and its first derivative with respect to time along the trajectories of (1), yields:

$$\dot{V} = s\dot{s} = s\left[\frac{di}{dt} - \frac{di^*}{dt}\right] \leq \frac{|s|}{L}\left[\left|-\upsilon - L\frac{di^*}{dt} + \frac{1}{2}E\right| - \frac{1}{2}E\right] < 0, \quad (16)$$

where (1) and (10) have been used, if $\left|-\upsilon - L\frac{di^*}{dt} + \frac{1}{2}E\right| - \frac{1}{2}E < 0$. By taking into account the two alternatives $-\upsilon - L\frac{di^*}{dt} + \frac{1}{2}E > 0$ and $-\upsilon - L\frac{di^*}{dt} + \frac{1}{2}E < 0$, is to show that (16) implies (15). It is stressed that (15) can always be satisfied in practice by selecting E accordingly to the task to be performed. With the sliding condition $\dot{s} = 0$, the dynamics (1), and condition (15); it is found that the following bound is satisfied by the equivalent control:

$$0 < u_{1eq} = \frac{1}{E}\left[\upsilon + L\frac{di^*}{dt}\right] < 1$$

which indicates that the system is capable of reaching the sliding regime. Additionally, equation (16) guarantees the achievement of the sliding surface $s = i - i^* = 0$, meaning that $i = i^*$ is attained. Therefore, the focus is on analyzing that dynamics (2)-(4) be stable when the closed-loop system, governed by (11)-(14), is evaluated at $i = i^*$.

B. CLOSED-LOOP DYNAMICS ON THE SLIDING SURFACE

Using $i = i^*$, $u_2 = zat(\overline{v})$, and (11) in (2), introducing and subtracting the terms $\bar{i}_a zat(\overline{v})$, $C\frac{d}{dt}[\overline{v}zat(\overline{v})]$, and $\frac{1}{k_m}(B\overline{\omega}_d + T_L)zat(\overline{v})$, and using the expression for $\bar{i}_a$ from equation (13), the constants can be redefined as $k_{p2} = k_p/k_m$ and $k_{i2} = k_i/k_m$. This leads to the following modified equations:

$$C\dot{e} = -\left(\frac{1}{R} + k_{p1}\right)e - k_{i1}\zeta + e_a zat(\overline{v}) + \frac{k_i}{k_m}\xi zat(\overline{v}) + C\frac{d\overline{v}}{dt}zat(\overline{v}) + C\overline{v}\frac{dzat(\overline{v})}{dt}, \quad (17)$$

$$\zeta = \int_0^t e(\tau)d\tau - \frac{1}{k_m k_{i1}}(B\overline{\omega}_d + T_L)zat(\overline{v}), \quad (18)$$

$$\xi = \int_0^t \tilde{\omega}(\tau)d\tau - \frac{1}{k_i}(B\overline{\omega}_d + T_L), \quad (19)$$

where:

$$\frac{d\overline{v}}{dt} = -r_a\dot{e}_a + \frac{R_a k_i}{k_m}\tilde{\omega} - \gamma e_a + \frac{fk_p}{k_m}\dot{\tilde{\omega}}, \quad (20)$$

$$C\overline{v}\frac{d\ zat(\overline{v})}{dt} = 0, \text{ if } |\bar{v}| \geq \beta_0 + \mu,$$

$$\left|C\overline{v}\frac{d\ zat(\overline{v})}{dt}\right| \leq C|\bar{v}|\ |\dot{\bar{v}}|\frac{M}{\beta_0} < C|\dot{\bar{v}}|(\beta_0 + \mu)\frac{M}{\beta_0} = C(1 + \alpha_0)|\dot{\bar{v}}|, \text{ if } |\bar{v}| < \beta_0 + \mu,$$

and (5), (6), $M = 1$ and the chain rule have been employed. After adding and subtracting terms $\overline{v}$, $k_e\omega_d$, $L_a\frac{d\bar{i}_a}{dt}$ in (3), using (13), $\omega_d(t) = \omega_d^*(t) + \overline{\omega}_d$, $k_{p2} = k_p/k_m$, $k_{i2} = k_i/k_m$, and defining $r = R_a + r_a$, $e_a = \rho + \sigma$ it is possible to write:

$$L_a\dot{\rho} = \frac{1}{2}[\upsilon zat(\bar{v}) - \bar{v}] - r\rho - \gamma z_1 + k_e\tilde{\omega} - \frac{1}{2}k_e\omega_d^*,$$

$$L_a\dot{\sigma} = \frac{1}{2}[\upsilon zat(\bar{v}) - \bar{v}] - r\sigma - \gamma z_2 + f_1\tilde{\omega} - \frac{1}{2}k_e\omega_d^*,$$

$$z_1 = \int_0^t \rho(\tau)d\tau + \frac{1}{2\gamma}k_e\overline{\omega}_d,\ z_2 = \int_0^t \sigma(\tau)d\tau + \frac{1}{2\gamma}k_e\overline{\omega}_d,$$

$$f_1 = f\frac{k_p}{k_m} - L_a\frac{k_i}{k_m} > 0.$$

After adding and subtracting the terms $J\dot{\omega}_d$, $k_m\bar{i}_a$, $B\omega_d$ in (4), using $\bar{i}_a$ defined in (13), $\omega_d(t) = \omega_d^*(t) + \overline{\omega}_d$, and $e_a = \rho + \sigma$

the following can be written:

$$J\dot{\tilde{\omega}} = -k_m\rho - k_m\sigma - k_i\xi - B\tilde{\omega} + J\dot{\omega}_d + B\omega_d^*, \quad (21)$$

with ξ defined in (19). Thus, the dynamics of the closed-loop system on the sliding surface $s = 0$ can be described by equations (17)–(21), and the state variables of such dynamics can be represented as $y_s = [\tilde{\omega}, \xi, \sigma, \rho, z_2, z_1, e, \zeta]^T$.

C. STABILITY ANALYSIS ON THE SLIDING SURFACE

The scalar function:

$$\begin{aligned} W(y_s) &= W_1(\tilde{\omega}, \xi) + W_2(\rho, z_1) + W_3(e, \zeta) \\ &\quad + W_4(\sigma, z_2), \quad (22)\\ W_1(\tilde{\omega}, \xi) &= \frac{1}{2}J\tilde{\omega}^2 + \alpha J\tilde{\omega}\xi + \frac{1}{2}k_i\xi^2,\\ W_2(\rho, z_1) &= \frac{1}{2}L_a\rho^2 + pL_az_1\rho + \frac{1}{2}\gamma z_1^2,\\ W_3(e, \zeta) &= \frac{1}{2}Ce^2 + \delta Ce\zeta + \frac{1}{2}k_{i1}\zeta^2,\\ W_4(\sigma, z_2) &= \frac{1}{2}L_a\frac{k_m}{f_1}\sigma^2 + \beta L_az_2\sigma + \frac{1}{2}\gamma\frac{k_m}{f_1}z_2^2, \end{aligned}$$

is positive definite and radially unbounded if $\alpha > 0$, $\overline{k}_i = k_i - \alpha^2 J > 0$, $p > 0$, $\overline{\gamma} = \gamma - p^2L_a > 0$, $\delta > 0$, $\overline{k}_{i1} = k_{i1} - \delta^2 C > 0$, $\beta > 0$, and $f_1 = \frac{p}{\beta}k_m$ are satisfied. Note that, based on Definition 2.1:

$$|\upsilon zat(\bar{\upsilon}) - \bar{\upsilon}| = |e|, \text{ if } |\bar{\upsilon}| \geq \beta_0 + \mu, \quad (23)$$

$$|\upsilon zat(\bar{\upsilon}) - \bar{\upsilon}| \leq |\upsilon| + |\bar{\upsilon}|, \text{ if } |\bar{\upsilon}| < \beta_0 + \mu, \quad (24)$$

and, according to (18), (5), and (6):

$$\dot{\zeta} = e, \text{ if } |\bar{\upsilon}| \geq \beta_0 + \mu, \quad (25)$$

$$|\dot{\zeta}| \leq |e| + \left|\frac{1}{k_mk_{i1}}(B\overline{\omega}_d + T_L)\right|\frac{1}{\beta_0}, \text{ if } |\bar{\upsilon}| < \beta_0 + \mu. \quad (26)$$

Consequently, after performing some cancelations and considering that $\pm qw \leq |q|\,|w|, \forall q, w \in \mathcal{R}$, $\|h\|_1 \leq \sqrt{n}\|h\|_2$, $\forall h \in \mathcal{R}^n$, and $|zat(\bar{\upsilon})| \leq M = 1$, it is observed that the first derivative of W with respect to time, previously given, along the trajectories associated with the closed-loop system over the sliding surface $s = 0$, i.e., equations (17)-(21), can be bounded as:

$$\dot{W} \leq -y^TQy + \|y\|\,|x|, \quad \text{if } |\bar{\upsilon}| \geq \beta_0 + \mu, \quad (27)$$

or:

$$\begin{aligned} \dot{W} \leq\ & -y^TQy + \|y\|\,|x| + (\delta C|e| \\ & + k_{i1}\zeta)\left|\frac{1}{k_mk_{i1}}(B\overline{\omega}_d + T_L)\right|\frac{1}{\beta_0} \\ & + \frac{1}{2}\left(\rho + pz_1 + \frac{k_m}{f_1}\sigma + \beta z_2\right)(|\upsilon| + |\bar{\upsilon}|), \\ & \text{if } |\bar{\upsilon}| < \beta_0 + \mu, \quad (28) \end{aligned}$$

being $y = [|\tilde{\omega}|, |\xi|, |\sigma|, |\rho|, |z_2|, |z_1|, |e|, |\zeta|]^T$, x is a scalar and bounded function of $\dot{\omega}_d$ and is equal to zero when $\dot{\omega}_d = 0$, whereas Q represents a symmetric matrix of dimension 8×8 whose entries are defined as:

$$\begin{aligned} Q_{11} &= B - \alpha J, \quad Q_{22} = \alpha k_i,\\ Q_{33} &= r\frac{k_m}{f_1} - \beta L_a, \quad Q_{44} = r - pL_a,\\ Q_{55} &= \beta\gamma, \quad Q_{66} = p\gamma,\\ Q_{77} &= \left(\frac{1}{R} + k_{p1}\right) - \frac{C(2+\alpha_0)r_a}{L_a} - \delta C,\\ Q_{88} &= \delta k_{i1},\\ Q_{13} &= Q_{31} = Q_{41} = Q_{14} = Q_{52} = Q_{25} = Q_{62}\\ &= Q_{26} = Q_{43} = Q_{34} = 0,\\ Q_{54} &= Q_{45} = Q_{63} = Q_{36} = Q_{65} = Q_{56} = 0,\\ Q_{12} &= Q_{21} = -\frac{\alpha B}{2}, \quad Q_{15} = Q_{51} = -\frac{\beta f_1}{2},\\ Q_{16} &= Q_{61} = -\frac{pk_e}{2},\\ Q_{17} &= Q_{71}\\ &= -\frac{C(2+\alpha_0)r_a}{2L_a}\left[\frac{fk_p}{k_m} + k_e + \frac{L_ak_i}{k_m}\right]\\ &\quad - \frac{C(2+\alpha_0)R_ak_i}{2k_m} - \frac{C(2+\alpha_0)fk_pB}{2Jk_m},\\ Q_{18} &= Q_{81} = \delta Q_{71}, \quad Q_{32} = Q_{23} = Q_{42}\\ &= Q_{24} = -\frac{\alpha k_m}{2},\\ Q_{72} &= Q_{27} = -\frac{k_i}{2k_m}\left[1 + \frac{C(2+\alpha_0)fk_p}{J}\right],\\ Q_{82} &= Q_{28} = \delta Q_{27},\\ Q_{53} &= Q_{35} = -\frac{\beta r}{2}, \quad Q_{73} = Q_{37}\\ &= -\frac{k_m}{4f_1} - \frac{C(2+\alpha_0)r_ar}{2L_a} - \frac{1}{2} - \frac{C(2+\alpha_0)fk_p}{2J}\\ &\quad - \frac{\gamma C(2+\alpha_0)}{2},\\ Q_{83} &= Q_{38} = \delta\left(Q_{73} + \frac{k_m}{4f_1}\right), \quad Q_{64} = Q_{46} = -\frac{pr}{2},\\ Q_{74} &= Q_{47} = Q_{37} - \frac{1}{4} + \frac{k_m}{4f_1}, \quad Q_{84} = Q_{48}\\ &= \delta\left(Q_{47} + \frac{1}{4}\right),\\ Q_{75} &= Q_{57} = -\frac{C(2+\alpha_0)r_a\gamma}{2L_a} - \frac{\beta}{4}, \quad Q_{85} = Q_{58}\\ &= -\frac{C(2+\alpha_0)r_a\gamma\delta}{2L_a},\\ Q_{76} &= Q_{67} = -\frac{C(2+\alpha_0)r_a\gamma}{2L_a} - \frac{p}{4}, \quad Q_{86} = Q_{68}\\ &= -\frac{C(2+\alpha_0)r_a\gamma\delta}{2L_a},\\ Q_{78} &= Q_{87} = -\frac{\delta}{2}\left(\frac{1}{R} + k_{p1}\right) - \frac{C(2+\alpha_0)r_a\delta}{2L_a}. \quad (29) \end{aligned}$$

The positivity of the eight principal minors of matrix Q are achieved through the following choices of parameters. The

corresponding first principal minor can be made positive by selecting $\alpha > 0$ sufficiently small due to the positivity of B. Whereas, the second principal minor can be made positive by choosing a large enough $k_i > 0$. To make the third principal minor positive, $r > 0$ must be chosen sufficiently large and $\beta > 0$ must be chosen small enough. Similarly, the fourth principal minor can be made positive by selecting a large enough value $r > 0$ and a small enough value $p > 0$. For the fifth and sixth principal minors, choosing a sufficiently large $\gamma > 0$ with any $f_1 > 0$ is sufficient. The seventh principal minor remains consistently positive when a sufficiently large $k_{p1} > 0$ is selected, while the eighth principal minor can be rendered positive by choosing $k_{i1} > 0$ large enough and $\delta > 0$ small enough. Therefore, guaranteeing $\lambda_{min}(Q) > 0$ is consistently achievable.

On the other hand, note that the terms:

$$(\delta C|e| + k_{i1}\zeta)\left|\frac{1}{k_m k_{i1}}(B\overline{\omega}_d + T_L)\right|\frac{1}{\beta_0} + \frac{1}{2}\left(\rho + pz_1 + \frac{k_m}{f_1}\sigma + \beta z_2\right)(|\upsilon| + |\bar{\upsilon}|), \tag{30}$$

in (28) might complicate the stability analysis when $|\bar{\upsilon}| < \beta_0 + \mu$. However, from the definition of $\bar{\upsilon}$ and $\bar{i}_a$ in (13) and e_a and $\tilde{\omega}$ in (14), it can be concluded that $|\bar{\upsilon}| \geq \beta_0 + \mu$ will become true for all $t > t_T$ for some finite $t_T \geq 0$, if $|\omega_d| > 0$ is large enough to demand a steady state value for $\bar{\upsilon}$ such that $|\bar{\upsilon}| \geq \beta_0 + \mu$. Thus, it can be assumed that (27) is the only case to be analyzed which, for some $0 < \Theta < 1$, can be written as:

$$\begin{aligned}\dot{W} &\leq -\lambda_{min}(Q)\|y_s\|^2 + \|y_s\|\,|x|,\\ &\leq -(1-\Theta)\lambda_{min}(Q)\|y_s\|^2, \quad \forall\, \|y_s\| \geq \frac{|x|}{\Theta\lambda_{min}(Q)}.\end{aligned} \tag{31}$$

D. PROOF OF PROPOSITION 3.1

Note that functions $W_j(\cdot,\cdot)$, for $j = 1,\ldots,4$, given in (22), are quadratic forms. Hence, there exist two class $\mathcal{K}_\infty$ functions $\alpha_1(\|y_s\|)$, $\alpha_2(\|y_s\|)$, that satisfy $\alpha_1(\|y_s\|) \leq W(y_s) \leq \alpha_2(\|y_s\|)$. This and (31), after using the Theorem 4.18 in [67] (pp. 172), indicate the boundedness and convergence of $y_s \in \mathcal{R}^8$ to a ball, the size of which relies on the upper limit of $|x|$, a scalar function of time. Furthermore, since $\omega_d(t_f) = \overline{\omega}_d$ for all $t \geq t_f$, where $t_f > 0$ is a finite value, means that $\omega_d^*(t) = 0$ and $\dot{\omega}_d(t) = 0$ for all $t \geq t_f$. Consequently, $|x(t)| = 0$ for all $t \geq t_f$, as mentioned before equation (29). This guarantees that $y_s \to 0$ as t approaches infinity. Thus, the proof of proposition 3.1 is complete.

It is emphasized that conditions guaranteeing the previously result are $\alpha > 0$, $\overline{k}_i = k_i - \alpha^2 J > 0$, $p > 0$, $\overline{\gamma} = \gamma - p^2 L_a > 0$, $\delta > 0$, $\overline{k}_{i1} = k_{i1} - \delta^2 C > 0$, $\beta > 0$, $f_1 = \frac{p}{\beta}k_m$ and appropriately selecting $\alpha > 0$, $k_i > 0$, $r > 0$, $\beta > 0$, $r > 0$, $p > 0$, $\gamma > 0$, $k_{p1} > 0$, $k_{i1} > 0$ and $\delta > 0$ ensuring that the eight principal minors of matrix Q, as defined in (29), are greater than zero.

Remark 3.3: It is important to emphasize that despite the equalities $k_{p2} = k_p/k_m$ and $k_{i2} = k_i/k_m$ introduced earlier in equation (17), it is not necessary to have precise knowledge of the exact value of k_m. However, k_p and k_i must satisfy the conditions of stability previously mentioned; yet, this does not demand a precise value for k_m. Therefore, both expressions $k_{p2} = k_p/k_m$ and $k_{i2} = k_i/k_m$ can be satisfied by utilizing sufficiently large values for k_{p2}, k_{i2}, and the other gains of the controller. Furthermore, regarding the first equality in equation (13), it is stated that the value of the armature resistance R_a needs to be precisely known. Nonetheless, this necessity can be relaxed by selecting a large enough controller gain r_a such that $r_a \gg R_a$, meaning that $r \approx r_a$. Analogously, the requirement for exact knowledge of the Buck converter output resistance R, as stated in equation (11), can be eased by choosing a large controller gain k_{p1}. Moreover, as discussed in Remark 3.2, this control is expected to exhibit robustness, allowing for compensation of uncertainties in both R_a and R via the PI controllers, which operate based on the error in converter output voltage and the electric current of the motor armature. Experimental results presented in Section IV provide confirmation of these observations.

Remark 3.4: Although it may initially appear cumbersome to verify the positivity of all the principal minors of matrix Q (as shown in equation (29)), it must be noted that the process is actually straightforward. The positiveness of each principal minor of Q is verified by the diagonal elements of Q. Therefore, ensuring the positivity of the $(i-1)$-th principal minor (keeping in mind that the first principal minor, Q_{11}, is a scalar) and selecting a sufficiently large value for the controller gain associated with Q_{ii} can render Q_{ii} positive. This procedure is iterated until the eighth principal minor is also established as positive.

IV. EXPERIMENTAL RESULTS

Here, experimental tests are conducted to provide an understanding of the performance achievable with the proposed approach presented in Proposition 3.1. These experiments were conducted using a MIMO "DC/DC Buck converter–inverter–DC motor" system, which was constructed at the Laboratorio de Mecatrónica y Energía Renovable at CIDETEC-IPN, México.

Fig. 3 depicts a block diagram showing relationship among hardware and software components employed to perform experimental tests. This block diagram is made up of three parts which are detailed in the following.

- *MIMO "DC/DC Buck converter–inverter–DC motor" system.* This part is composed by the plant to be controlled, i.e., the MIMO "DC/DC Buck converter–inverter–DC motor" system. The measure of currents i and i_a are realized through Tektronix A622 current probes. Voltage signals υ and ϑ are acquired by using two Tektronix P5200A voltage probes. Velocity ω measurements are performed using an Omron E6B2-CWZ6C encoder. A permanent magnet brushed DC motor model GNM 5440E-G3.1 from Engel was

employed. The nominal parameters of the MIMO system prototype under study are the following:

$$\begin{aligned} &E = 45\ \text{V}, \quad R = 61.8\ \Omega, \\ &C = 114.4\ \mu\text{F}, \quad L = 4.94\ \text{mH}, \\ &L_a = 2.22\ \text{mH}, \quad k_m = 120.1 \times 10^{-3}\ \tfrac{\text{N·m}}{\text{A}}, \\ &R_a = 0.965\ \Omega, \quad k_e = 120.1 \times 10^{-3}\ \tfrac{\text{V·s}}{\text{rad}}, \\ &J = 118.2 \times 10^{-3}\ \text{kg}\cdot\text{m}^2, \quad B = 129.6 \times 10^{-3}\ \tfrac{\text{N·m·s}}{\text{rad}}. \end{aligned} \tag{32}$$

- *Bidirectional tracking robust control*. Control strategy presented in Proposition 3.1 is implemented in this part using Matlab-Simulink. The *desired velocity trajectory* ω_d is also computed here.
- *Controller board and signal conditioning*. Here, the connections between the prototype and the DS1104 board are shown. Control signal $\bar{u}_1$ is computed in this block. This signal is applied to experimental prototype, using the DS1104 board digital I/O signals, at the NTE3087 in order to turn-on and turn-off transistor of the Buck converter. The control signal u_2 is processed in the "signal rescaling" block (interprets $u_2 = -1$ as $u_2 = 0$) and through a NOT logic gate the control signal $\bar{u}_2$ is obtained. This pair of signals (i.e., u_2 and $\bar{u}_2$) are then applied to circuits TLP250 and drivers IR2113 in order to turn-on and turn-off transistors of the full bridge inverter. On the other hand, i_a, υ, i, and θ are processed by the signal conditioning (SC) blocks. Finally, within this block the velocity ω is also computed by numeric differentiation of angular position, θ, which is obtained directly from the E6B2-CWZ6C encoder.

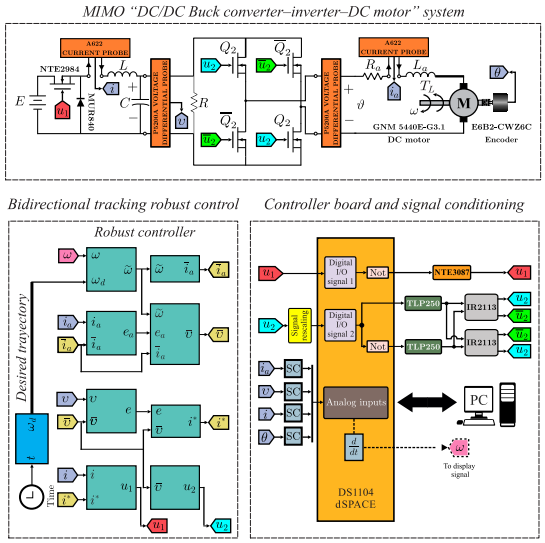

FIGURE 3. Block diagram of the closed-loop system.

Fig. 4 illustrates the hardware configuration of the MIMO "DC/DC Buck converter–inverter–DC motor" system when operated in closed-loop control. The system includes the following components: 1) power supply E, 2) personal computer, 3) DS1104 board from dSPACE, 4) Tektronix P5200A voltage probe, 5) Tektronix A622 current probe, 6) DC/DC-Buck converter, 7) full-bridge inverter, 8) encoder, and 9) Engel GNM 5440E-G3.1 DC motor.

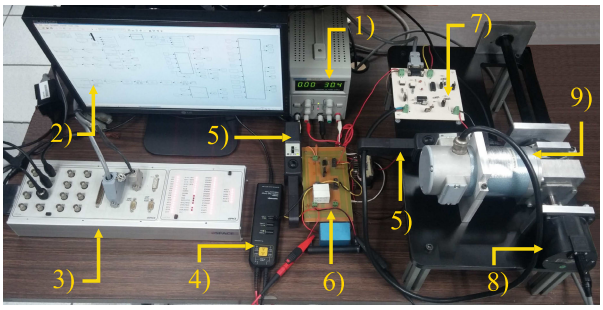

FIGURE 4. Picture of prototype used in experiments.

The controller gains employed for (10)-(14) are $k_{p1} = 29$, $k_{i1} = 2$, $k_{p2} = 0.8326$, $k_{i2} = 9.1590$, $f = 1$, $r_a = 0.5$, and $\gamma = 50$. The proposed desired velocity is described as follows:

$$\omega_d = \begin{cases} \overline{\omega}_{i_1}(t_{i_1}) + [\overline{\omega}_{f_1}(t_{f_1}) - \overline{\omega}_{i_1}(t_{i_1})]\varphi_1\left(t, t_{i_1}, t_{f_1}\right) \\ \qquad\qquad\qquad\qquad t \le 5\ \text{s}, \\ \overline{\omega}_{i_2}(t_{i_2}) + [\overline{\omega}_{f_2}(t_{f_2}) - \overline{\omega}_{i_2}(t_{i_2})]\varphi_2\left(t, t_{i_2}, t_{f_2}\right) \\ \qquad\qquad\qquad\qquad t > 5\ \text{s}, \end{cases} \tag{33}$$

where $\varphi_1\left(t, t_{i_1}, t_{f_1}\right)$ and $\varphi_2\left(t, t_{i_2}, t_{f_2}\right)$ are Bézier polynomials defined as:

$$\varphi_1 = \begin{cases} 0 & t \le t_{i_1}, \\ \varsigma_1^5\,[252 - 1050\,\varsigma_1 + 1800\,\varsigma_1^2 - 1575\,\varsigma_1^3 \\ +700\,\varsigma_1^4 - 126\,\varsigma_1^5] & t \in (t_{i_1}, t_{f_1}), \\ 1 & t \ge t_{f_1}, \end{cases}$$

$$\varphi_2 = \begin{cases} 0 & t \le t_{i_2}, \\ \varsigma_2^5\,[252 - 1050\,\varsigma_2 + 1800\,\varsigma_2^2 - 1575\,\varsigma_2^3 \\ +700\,\varsigma_2^4 - 126\,\varsigma_2^5] & t \in (t_{i_2}, t_{f_2}), \\ 1 & t \ge t_{f_2}, \end{cases}$$

and $\varsigma_1 = \frac{t - t_{i_1}}{t_{f_1} - t_{i_1}}$, $\varsigma_2 = \frac{t - t_{i_2}}{t_{f_2} - t_{i_2}}$. This ensures that ω_d smoothly interpolates from the initial velocity $\overline{\omega}_{i_1}$ to the final velocity $\overline{\omega}_{f_1}$ in the time interval $[t_{i_1}, t_{f_1}]$. After this, ω_d smoothly interpolates from the initial velocity $\overline{\omega}_{i_2}$ and the final velocity $\overline{\omega}_{f_2}$ in the time interval $[t_{i_2}, t_{f_2}]$. All initial and final times are defined for each experiment that follows.

A. EXPERIMENT NUMBER 1: NOMINAL VALUES

In the first experimental test the trajectory tracking capabilities of the developed control scheme is shown, when the system nominal values (32) are considered. With this aim, the following parameters were considered $t_{i_1} = 0$ s, $t_{f_1} = 1.5$ s, $t_{i_2} = 8$ s, $t_{f_2} = 13$ s, $\overline{\omega}_{i_1} = 0\ \frac{\text{rad}}{\text{s}}$, $\overline{\omega}_{f_1} = 13\ \frac{\text{rad}}{\text{s}}$, $\overline{\omega}_{i_2} = 13\ \frac{\text{rad}}{\text{s}}$, and $\overline{\omega}_{f_2} = -13\ \frac{\text{rad}}{\text{s}}$ in order to define the desired trajectory in (33). These results are plotted in Figs. 5 and 6.

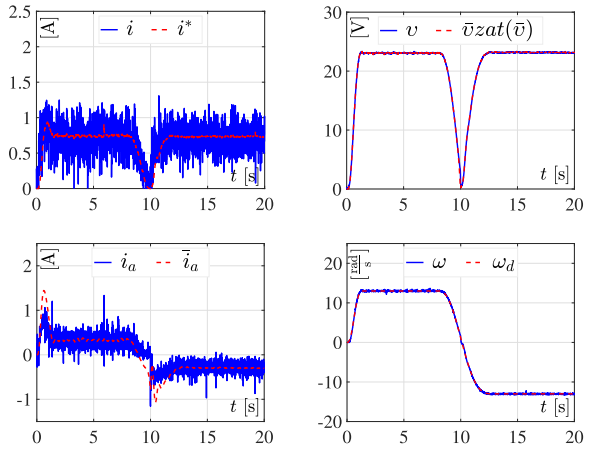

FIGURE 5. Experiment number 1: Closed-loop system variables when nominal values (32) are considered.

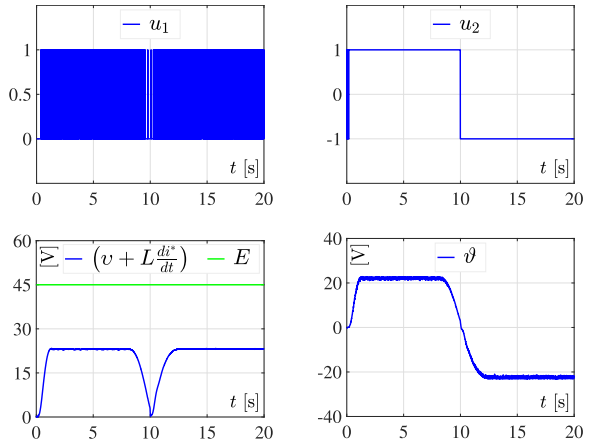

FIGURE 6. Experiment number 1: Switched control signals, sliding condition, and voltage at the DC motor terminals when nominal values (32) are considered.

Note that the actual velocity ω tracks very well the desired velocity ω_d both signals overlap all the time. Note that voltage at motor terminals ϑ is a smooth signal. This is important to highlight because it verifies that the main purpose to construct and control the MIMO "DC/DC Buck converter–inverter–DC motor" system has been accomplished: a PWM voltage is not applied at motor terminals but a voltage signal whose magnitude smoothly varies to allow motor to reach the time varying desired velocity. Recall that $\vartheta = \upsilon u_2$. Hence, a smooth ϑ is ensured by a smooth voltage at the converter capacitor υ (excepting at $\upsilon = 0$) and a piece wise continuous signal u_2. This property on u_2 might be lost if motor velocity is constant at zero without an applied load torque.

Recall definitions $e = \bar{\upsilon}zat(\bar{\upsilon}) - \upsilon$, $\vartheta = \upsilon u_2$ and $u_2 = zat(\bar{\upsilon})$. This means that $\upsilon = \vartheta$ if both $\vartheta > 0$ and $u_2 > 0$, whereas $\upsilon = -\vartheta$ if both $\vartheta < 0$ and $u_2 < 0$. See Fig. 5. On the other hand, since $\upsilon \geq 0$ under normal operation conditions of the converter, the desired value for υ is $\bar{\upsilon}zat(\bar{\upsilon})$ which is always positive or zero. This explains why, in Fig. 5, $\bar{\upsilon}zat(\bar{\upsilon}) = \upsilon$ all the time.

It is observed that the SMC enforces the electric current i to achieve, in an average sense, its desired value i^*. However, the sliding mode is lost (see plot of u_1) at $t = 10$ s, i.e., when $\omega = \omega_d = 0$. This happens because the sliding condition in (15) is not satisfied, i.e., $\upsilon + L\frac{di^*}{dt} = 0$ at $t = 10$ s. Moreover, recall that, in paragraph after (30), it is stated that some performance problems might appear if $|\omega_d| > 0$ is not large enough, which is particularly true if $\omega_d = 0$. Finally, it is also observed that $i_a \to \bar{i}_a$.

B. EXPERIMENT NUMBER 2: TORQUE DISTURBANCE

Here, the same parameters as in Experiment number 1 to define trajectory in (33) were used. Also, a torque disturbance T_L is considered which is applied by means of a brake system acting on motor which is applied in the time interval $t \in$ [5 s, 16 s]. These results are shown in Figs. 7 and 8.

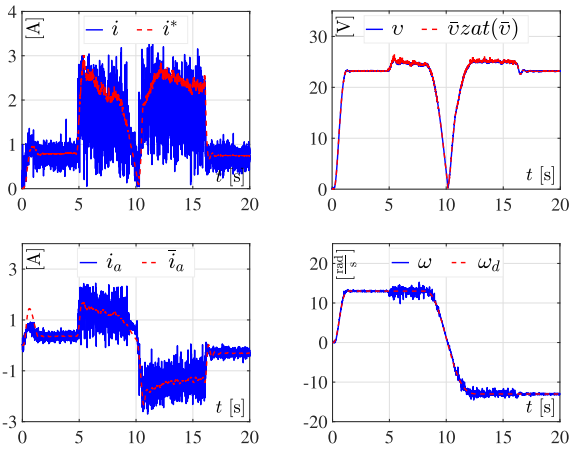

FIGURE 7. Experiment number 2: Closed-loop system variables when a torque disturbance is applied.

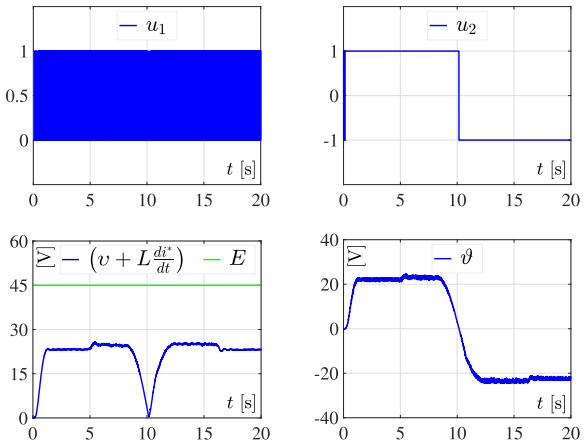

FIGURE 8. Experiment number 2: Switched control signals, sliding condition, and voltage at DC motor terminals when a torque disturbance is applied.

It can be seen that velocity tracking is very good since the actual velocity overlaps the desired velocity all the time. Note that measured velocity becomes a little noisy when torque disturbance is applied. Also, note that all voltages and electric currents are affected when torque disturbance appears. However, voltage ϑ at motor terminals remains a smooth signal instead of a PWM signal. Finally,

the sliding condition in (15) is met again, except for around $t = 10$ s.

C. EXPERIMENT NUMBER 3: FASTER CHANGES IN MOTOR MOVEMENT

The intention of the third experiment is to command a faster change in the desired velocity. This is performed when commanding a reversal change in the desired velocity. With this aim, the following parameters are considered $t_{i_1} = 0$ s, $t_{f_1} = 1.5$ s, $t_{i_2} = 10$ s, $t_{f_2} = 11.5$ s, $\overline{\omega}_{i_1} = 0 \frac{\text{rad}}{\text{s}}$, $\overline{\omega}_{f_1} = 13 \frac{\text{rad}}{\text{s}}$, $\overline{\omega}_{i_2} = 13 \frac{\text{rad}}{\text{s}}$, and $\overline{\omega}_{f_2} = -13 \frac{\text{rad}}{\text{s}}$ in order to define the desired trajectory in (33). The obtained results are shown in Figs. 9 and 10.

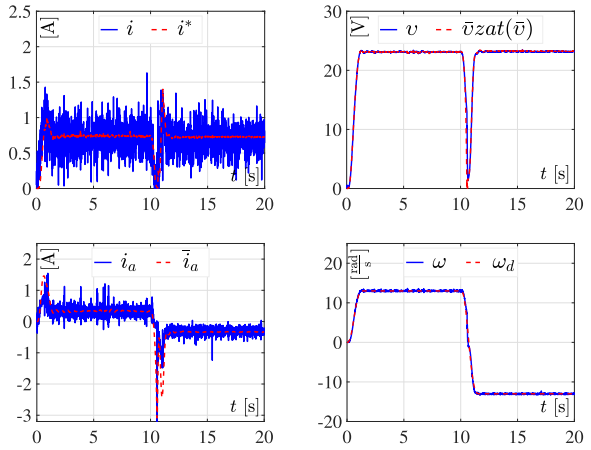

FIGURE 9. Experiment number 3: Closed-loop system variables when a faster reference change ω_d is considered.

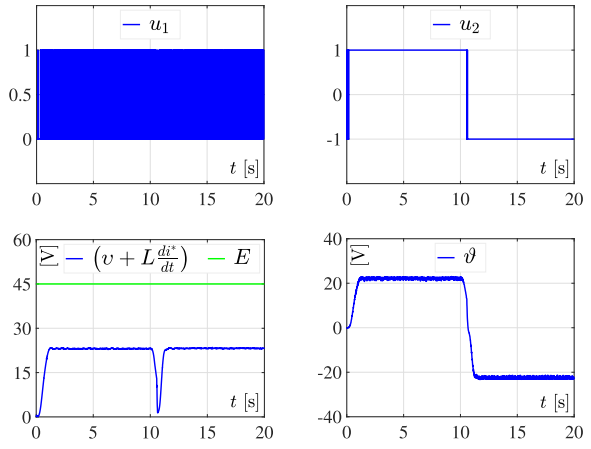

FIGURE 10. Experiment number 3: Switched control signals, sliding condition, and voltage at DC motor terminals, when a faster reference change ω_d is considered.

Note that the actual velocity overlaps the desired velocity all the time. Hence, tracking performance is very good again. It is realized that all of the other variables behave similarly as in the previous experiments. The important thing in the third experiment is that the sliding mode is not lost. This can be seen in the plot of u_1 and in the plot of $v + L\frac{di^*}{dt}$ which is always greater than 0 and less than 1. This means that the sliding condition in (15) is always satisfied.

D. EXPERIMENTS UNDER PARAMETRIC UNCERTAINTIES IN R, E, AND C

Figs. 11–16, present the experimental results when parametric uncertainties exist in R, E, C, alone, respectively. The parametric uncertainties that appear in each one of these figures are introduced according to the following.

$$\text{Figs. 11 and 12:} \quad R_p = \begin{cases} R, & 0\text{ s} \le t < 5\text{ s}, \\ 50\%R, & 5\text{ s} \le t < 16\text{ s}, \\ 200\%R, & 16\text{ s} \le t < 20\text{ s}, \\ R_\infty, & 20\text{ s} \le t \le 25\text{ s}. \end{cases}$$

$$\text{Figs. 13 and 14:} \quad E_p = \begin{cases} E, & 0\text{ s} \le t < 5\text{ s}, \\ 66\%E, & 5\text{ s} \le t < 16\text{ s}, \\ E, & 16\text{ s} \le t \le 20\text{ s}. \end{cases}$$

$$\text{Figs. 15 and 16:} \quad C_p = \begin{cases} C, & 0\text{ s} \le t < 5\text{ s}, \\ 450\%C, & 5\text{ s} \le t < 16\text{ s}, \\ C, & 16\text{ s} \le t \le 20\text{ s}. \end{cases}$$

Symbols R_p, E_p, and C_p, represent, respectively, the actual values that the converter resistance, the power supply voltage, and the converter capacitance take, whereas R, E, and C are the nominal values presented in (32) which are the known values for the controller. All of these experiments have employed the same parameters as in Experiment number 1 to define the desired velocity in (33).

One key highlight of the results presented in Figs. 11 and 12 is that considering the value of R_∞ in practice implies disconnecting R from the Buck converter. Based on the results in Fig. 11, it can be concluded that including or excluding R from the system under study is inconsequential. This is because, in both cases, the control objective is achieved (i.e., $\omega \to \omega_d$).

It can be observed in Figs. 11–16, that the main effects of all these parametric uncertainties appear on the electric

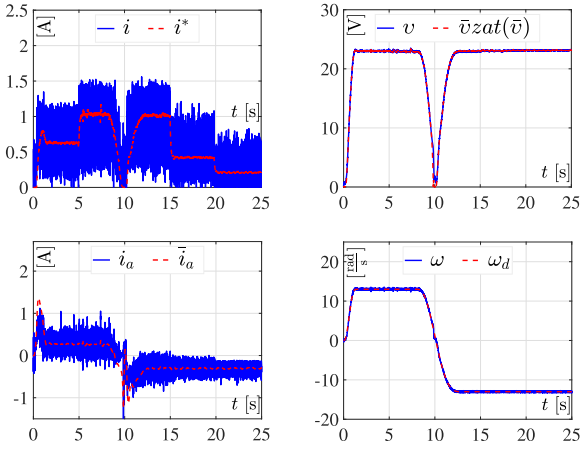

FIGURE 11. Parametric uncertainty in the converter resistance: Closed-loop system variables.

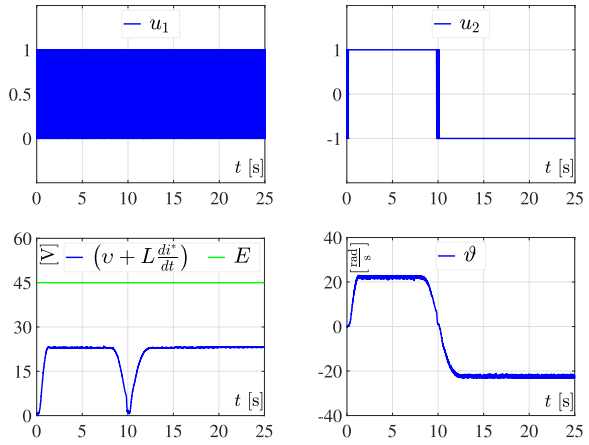

FIGURE 12. Parametric uncertainty in the converter resistance: Switched control signals, sliding condition, and voltage at DC motor terminals.

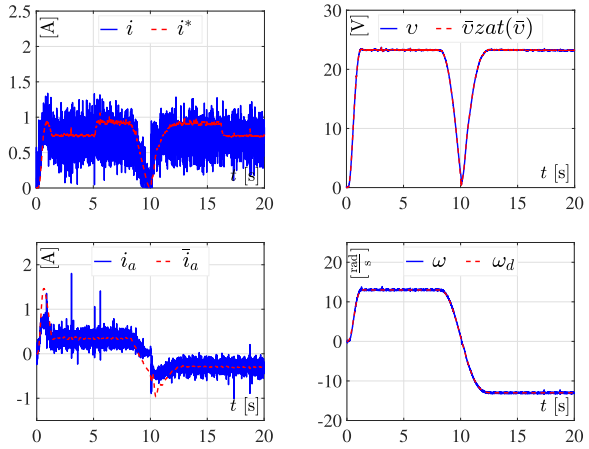

FIGURE 13. Parametric uncertainty in the power supply voltage: Closed-loop system variables.

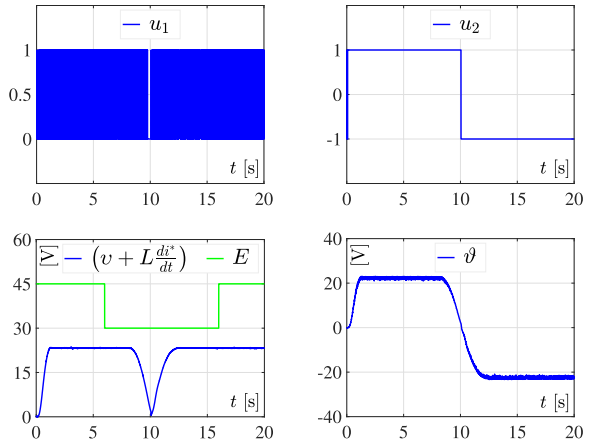

FIGURE 14. Parametric uncertainty in the power supply voltage: Switched control signals, sliding condition, and voltage at DC motor terminals.

current through the converter inductance and its corresponding desired profile. This means that all of these parametric uncertainties are compensated by the sliding modes part of the controller. This explains why motor velocity is not affected (aside from some noisy measurements from time to time) by these uncertainties in these experiments.

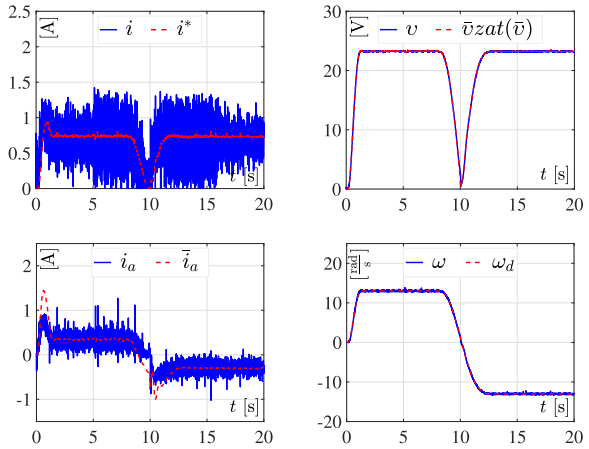

FIGURE 15. Parametric uncertainty in the converter capacitance: Closed-loop system variables.

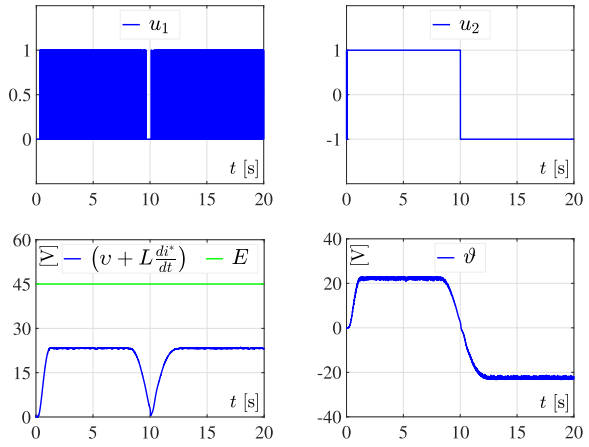

FIGURE 16. Parametric uncertainty in the converter capacitance: Switched control signals, sliding condition, and voltage at DC motor terminals.

V. CONCLUSION

In this paper, a controller is proposed for the MIMO "DC/DC Buck converter–inverter–DC motor" system. Such a system was previously proposed but abandoned due to the inability to deliver a smooth voltage signal at the DC motor terminals, instead of a pulse width modulation (PWM) signal. The study demonstrates that by appropriately designing the controller, a smooth voltage signal can indeed be achieved at the DC motor terminals. A formal proof of the asymptotic stability related to the closed-loop system is provided. The proposed controller incorporates multiple proportional-integral (PI) loops for velocity control, armature current control, and converter capacitor voltage control. Additionally, a sliding modes controller is employed for controlling the current through the converter inductor. Through experimental validation on a prototype system, the robustness against plant parameter uncertainty and external disturbances is verified for the proposed control scheme.

REFERENCES

[1] F. Antritter, P. Maurer, and J. Reger, "Flatness based control of a Buck-converter driven DC motor," in *Proc. 4th IFAC Symp. Mech. Syst.*, Heidelberg, Germany, 2006, vol. 39, no. 16, pp. 36–41, doi: 10.3182/20060912-3-DE-2911.00010.

[2] S. E. Lyshevski, *Electromechanical Systems, Electric Machines, and Applied Mechatronics*. Boca Raton, FL, USA: CRC Press, 2000.
[3] H. Sira-Ramírez and M. A. Oliver-Salazar, "On the robust control of Buck-converter DC-motor combinations," *IEEE Trans. Power Electron.*, vol. 28, no. 8, pp. 3912–3922, Aug. 2013, doi: 10.1109/TPEL.2012.2227806.
[4] R. Silva-Ortigoza, V. M. Hernández-Guzmán, M. Antonio-Cruz, and D. Muñoz-Carrillo, "DC/DC Buck power converter as a smooth starter for a DC motor based on a hierarchical control," *IEEE Trans. Power Electron.*, vol. 30, no. 2, pp. 1076–1084, Feb. 2015. [Online]. Available: https://ieeexplore.ieee.org/document/6767144
[5] G. K. Srinivasan and H. T. Srinivasan, "Sensorless load torque estimation and passivity based control of Buck converter fed DC motor," *Sci. World J.*, vol. 2015, pp. 1–15, Mar. 2015. [Online]. Available: https://www.hindawi.com/journals/tswj/2015/132843
[6] V. M. Hernández-Guzman, R. Silva-Ortigoza, and D. Muñoz-Carrillo, "Velocity control of a brushed DC-motor driven by a DC to DC Buck power converter," *Int. J. Innov. Comput., Inf. Control*, vol. 11, no. 2, pp. 509–521, 2015. [Online]. Available: http://www.ijicic.org/ijicic-110209.pdf
[7] T. K. Nizami, A. Chakravarty, and C. Mahanta, "Design and implementation of a neuro-adaptive backstepping controller for Buck converter fed PMDC-motor," *Control Eng. Pract.*, vol. 58, pp. 78–87, Jan. 2017, doi: 10.1016/j.conengprac.2016.10.002.
[8] S. W. Khubalkar, A. S. Junghare, M. V. Aware, A. S. Chopade, and S. Das, "Demonstrative fractional order—PID controller based DC motor drive on digital platform," *ISA Trans.*, vol. 82, pp. 79–93, Nov. 2018, doi: 10.1016/j.isatra.2017.08.019.
[9] F. E. Hoyos-Velasco, J. E. Candelo-Becerra, and A. Rincón-Santamaría, "Dynamic analysis of a permanent magnet DC motor using a Buck converter controlled by ZAD-FPIC," *Energies*, vol. 11, no. 12, Dec. 2018, Art. no. 3388, doi: 10.3390/en11123388.
[10] M. G. Kazemi and M. Montazeri, "Fault detection of continuous time linear switched systems using combination of bond graph method and switching observer," *ISA Trans.*, vol. 94, pp. 338–351, Nov. 2019, doi: 10.1016/j.isatra.2019.04.023.
[11] J. Yang, H. Wu, L. Hu, and S. Li, "Robust predictive speed regulation of converter-driven DC motors via a discrete-time reduced-order GPIO," *IEEE Trans. Ind. Electron.*, vol. 66, no. 10, pp. 7893–7903, Oct. 2019, doi: 10.1109/TIE.2018.2878119.
[12] F. E. Hoyos-Velasco, J. E. Candelo-Becerra, and C. I. Hoyos-Velasco, "Application of zero average dynamics and fixed point induction control techniques to control the speed of a DC motor with a Buck converter," *Appl. Sci.*, vol. 10, no. 5, Mar. 2020, Art. no. 1807, doi: 10.3390/app10051807.
[13] G. Rigatos, P. Siano, and M. Sayed-Mouchaweh, "Adaptive neurofuzzy H-infinity control of DC–DC voltage converters," *Neural Comput. Appl.*, vol. 32, no. 7, pp. 2507–2520, Apr. 2020, doi: 10.1007/s00521-019-04394-4.
[14] R. Madonski, K. Łakomy, M. Stankovic, S. Shao, J. Yang, and S. Li, "Robust converter-fed motor control based on active rejection of multiple disturbances," *Control Eng. Pract.*, vol. 107, Feb. 2021, Art. no. 104696, doi: 10.1016/j.conengprac.2020.104696.
[15] M. R. Stanković, R. Madonski, S. Shao, and D. Mikluc, "On dealing with harmonic uncertainties in the class of active disturbance rejection controllers," *Int. J. Control*, vol. 94, no. 10, pp. 2795–2810, Oct. 2021, doi: 10.1080/00207179.2020.1736639.
[16] A. Rauf, M. Zafran, A. Khan, and A. R. Tariq, "Finite-time nonsingular terminal sliding mode control of converter-driven DC motor system subject to unmatched disturbances," *Int. Trans. Electr. Energy Syst.*, vol. 31, no. 11, Nov. 2021, Art. no. e13070, doi: 10.1002/2050-7038.13070.
[17] L. Zhang, J. Yang, and S. Li, "A model-based unmatched disturbance rejection control approach for speed regulation of a converter-driven DC motor using output-feedback," *IEEE/CAA J. Autom. Sinica*, vol. 9, no. 2, pp. 365–376, Feb. 2022, doi: 10.1109/JAS.2021.1004213.
[18] E. Guerrero-Ramírez, A. Martínez-Barbosa, E. Guzmán-Ramírez, and J. L. Barahona-Ávalos, "Design methodology for digital active disturbance rejection control of the DC motor drive," *e-Prime-Adv. Elect. Eng., Electron. Energy*, vol. 2, Aug. 2022, Art. no. 100050. [Online]. Available: https://www.sciencedirect.com/science/article/pii/S2772671122000225
[19] E. Guerrero-Ramírez, A. Martínez-Barbosa, M. A. Contreras-Ordaz, G. Guerrero-Ramírez, E. Guzmán-Ramírez, J. L. Barahona-Avalos, and M. Adam-Medina, "DC motor drive powered by solar photovoltaic energy: An FPGA-based active disturbance rejection control approach," *Energies*, vol. 15, no. 18, Sep. 2022, Art. no. 6595, doi: 10.3390/en15186595.
[20] T. K. Nizami, A. Chakravarty, C. Mahanta, A. Iqbal, and A. Hosseinpour, "Enhanced dynamic performance in DC–DC converter-PMDC motor combination through an intelligent non-linear adaptive control scheme," *IET Power Electron.*, vol. 15, no. 15, pp. 1607–1616, Nov. 2022, doi: 10.1049/pel2.12330.
[21] D. Ravikumar and G. K. Srinivasan, "Implementation of higher order sliding mode control of DC–DC Buck converter fed permanent magnet DC motor with improved performance," *Automatika*, vol. 64, no. 1, pp. 162–177, Jan. 2023, doi: 10.1080/00051144.2022.2119499.
[22] A. Chouya, "Adaptive sliding mode control with chattering elimination for Buck converter driven DC motor," *WSEAS Trans. Syst.*, vol. 22, pp. 19–28, Feb. 2023, doi: 10.37394/23202.2023.22.3.
[23] M. D. Patil, K. Vadirajacharya, and S. W. Khubalkar, "Design and tuning of digital fractional-order PID controller for permanent magnet DC motor," *IETE J. Res.*, vol. 69, no. 7, pp. 4349–4359, Sep. 2023, doi: 10.1080/03772063.2021.1942243.
[24] J. Linares-Flores, J. Reger, and H. Sira-Ramírez, "Load torque estimation and passivity-based control of a Boost-converter/DC-motor combination," *IEEE Trans. Control Syst. Technol.*, vol. 18, no. 6, pp. 1398–1405, Nov. 2010, doi: 10.1109/TCST.2009.2037809.
[25] A. T. Alexandridis and G. C. Konstantopoulos, "Modified PI speed controllers for series-excited DC motors fed by DC/DC Boost converters," *Control Eng. Pract.*, vol. 23, pp. 14–21, Feb. 2014, doi: 10.1016/j.conengprac.2013.10.009.
[26] S. Malek, "A new nonlinear controller for DC–DC Boost converter fed DC motor," *Int. J. Power Electron.*, vol. 7, nos. 1–2, pp. 54–71, 2015, doi: 10.1504/IJPELEC.2015.071199.
[27] G. C. Konstantopoulos and A. T. Alexandridis, "Enhanced control design of simple DC–DC Boost converter-driven DC motors: Analysis and implementation," *Electr. Power Compon. Syst.*, vol. 43, no. 17, pp. 1946–1957, Oct. 2015, doi: 10.1080/15325008.2015.1070383.
[28] G. K. Srinivasan, H. T. Srinivasan, and M. Rivera, "Sensitivity analysis of exact tracking error dynamics passive output control for a flat/partially flat converter systems," *Electronics*, vol. 9, no. 11, Nov. 2020, Art. no. 1942, doi: 10.3390/electronics9111942.
[29] P. Mishra, A. Banerjee, M. Ghosh, and C. B. Baladhandautham, "Digital pulse width modulation sampling effect embodied steady-state time-domain modeling of a Boost converter driven permanent magnet DC brushed motor," *Int. Trans. Electr. Energy Syst.*, vol. 31, no. 8, Aug. 2021, Art. no. e12970, doi: 10.1002/2050-7038.12970.
[30] R. Silva-Ortigoza, A. Roldán-Caballero, E. Hernández-Márquez, R. E. García-Chávez, M. Marciano-Melchor, J. R. García-Sánchez, and G. Silva-Ortigoza, "Hierarchical flatness-based control for velocity trajectory tracking of the DC/DC Boost converter–DC motor' system powered by renewable energy," *IEEE Access*, vol. 11, pp. 32464–32475, Apr. 2023. [Online]. Available: https://ieeexplore.ieee.org/document/10078157
[31] Y. Sönmez, M. Dursun, U. Güvenç, and C. Yilmaz, "Start up current control of Buck-Boost convertor-fed serial DC motor," *Pamukkale Univ. J. Eng. Sci.*, vol. 15, no. 2, pp. 278–283, 2009.
[32] J. Linares-Flores, J. L. Barahona-Avalos, H. Sira-Ramírez, and M. A. Contreras-Ordaz, "Robust passivity-based control of a Buck-Boost-converter/DC-motor system: An active disturbance rejection approach," *IEEE Trans. Ind. Appl.*, vol. 48, no. 6, pp. 2362–2371, Nov. 2012, doi: 10.1109/TIA.2012.2227098.
[33] M. H. Arshad and M. A. Abido, "Hierarchical control of DC motor coupled with Cuk converter combining differential flatness and sliding mode control," *Arabian J. Sci. Eng.*, vol. 46, no. 10, pp. 9413–9422, Oct. 2021, doi: 10.1007/s13369-020-05305-9.
[34] G. K. Srinivasan, H. T. Srinivasan, and M. Rivera, "Low-cost implementation of passivity-based control and estimation of load torque for a Luo converter with dynamic load," *Electronics*, vol. 9, no. 11, Nov. 2020, Art. no. 1914, doi: 10.3390/electronics9111914.
[35] R. Silva-Ortigoza, J. N. Alba-Juárez, J. R. García-Sánchez, M. Antonio-Cruz, V. M. Hernández-Guzmán, and H. Taud, "Modeling and experimental validation of a bidirectional DC/DC Buck power electronic converter-DC motor system," *IEEE Latin Amer. Trans.*, vol. 15, no. 6, pp. 1043–1051, Jun. 2017, doi: 10.1109/TLA.2017.7932691.
[36] R. Silva-Ortigoza, J. N. Alba-Juárez, J. R. García-Sánchez, V. M. Hernández-Guzmán, C. Y. Sosa-Cervantes, and H. Taud, "A sensorless passivity-based control for the DC/DC Buck converter-inverter-DC motor system," *IEEE Latin Amer. Trans.*, vol. 14, no. 10, pp. 4227–4234, Oct. 2016, doi: 10.1109/TLA.2016.7786298.
[37] E. Hernández-Márquez, J. R. García-Sánchez, R. Silva-Ortigoza, M. Antonio-Cruz, V. M. Hernández-Guzmán, H. Taud, and M. Marcelino-Aranda, "Bidirectional tracking robust controls for a DC/DC Buck converter-DC motor system," *Complexity*, vol. 2018, pp. 1–10, Aug. 2018, Art. no. 1260743, doi: 10.1155/2018/1260743.

[38] X. Chi, S. Quan, J. Chen, Y.-X. Wang, and H. He, "Proton exchange membrane fuel cell-powered bidirectional DC motor control based on adaptive sliding-mode technique with neural network estimation," *Int. J. Hydrogen Energy*, vol. 45, no. 39, pp. 20282–20292, Aug. 2020, doi: 10.1016/j.ijhydene.2019.12.224.

[39] V. García-Rodríguez, R. Silva-Ortigoza, E. Hernández-Márquez, J. García-Sánchez, and H. Taud, "DC/DC Boost converter–inverter as driver for a DC motor: Modeling and experimental verification," *Energies*, vol. 11, no. 8, Aug. 2018, Art. no. 2044, doi: 10.3390/en11082044.

[40] R. Silva-Ortigoza, V. H. Gárcia-Rodríguez, E. Hernández-Márquez, M. Ponce, J. R. Gárcia-Sánchez, J. N. Alba-Juárez, G. Silva-Ortigoza, and J. H. Pérez, "A trajectory tracking control for a Boost converter-inverter-DC motor combination," *IEEE Latin Amer. Trans.*, vol. 16, no. 4, pp. 1008–1014, Apr. 2018, doi: 10.1109/TLA.2018.8362130.

[41] J. R. García-Sánchez, E. Hernández-Márquez, J. Ramírez-Morales, M. Marciano-Melchor, M. Marcelino-Aranda, H. Taud, and R. Silva-Ortigoza, "A robust differential flatness-based tracking control for the 'MIMO DC/DC Boost converter–inverter–DC motor' system: Experimental results," *IEEE Access*, vol. 7, pp. 84497–84505, Jul. 2019. [Online]. Available: https://ieeexplore.ieee.org/abstract/document/8740891

[42] E. Hernández-Márquez, R. Silva-Ortigoza, J. R. Gárcia-Sánchez, V. H. Gárcia-Rodríguez, and J. N. Alba-Juárez, "A new 'DC/DC Buck-Boost converter–DC motor' system: Modeling and experimental validation," *IEEE Latin Amer. Trans.*, vol. 15, no. 11, pp. 2043–2049, Nov. 2017, doi: 10.1109/TLA.2017.8070406.

[43] E. Hernández-Márquez, R. Silva-Ortigoza, J. R. García-Sánchez, M. Marcelino-Aranda, and G. Saldaña-González, "A DC/DC Buck-Boost converter–inverter–DC motor system: Sensorless passivity-based control," *IEEE Access*, vol. 6, pp. 31486–31492, 2018. [Online]. Available: https://ieeexplore.ieee.org/document/8382160

[44] E. Hernández-Márquez, C. Avila-Rea, J. García-Sánchez, R. Silva-Ortigoza, G. Silva-Ortigoza, H. Taud, and M. Marcelino-Aranda, "Robust tracking controller for a DC/DC Buck-Boost converter–inverter–DC motor system," *Energies*, vol. 11, no. 10, Oct. 2018, Art. no. 2500, doi: 10.3390/en11102500.

[45] M. R. Ghazali, M. A. Ahmad, and R. M. T. R. Ismail, "Adaptive safe experimentation dynamics for data-driven neuroendocrine-PID control of MIMO systems," *IETE J. Res.*, vol. 68, no. 3, pp. 1611–1624, May 2022, doi: 10.1080/03772063.2019.1656556.

[46] J. Linares-Flores, H. Sira-Ramírez, E. F. Cuevas-López, and M. A. Contreras-Ordaz, "Sensorless passivity based control of a DC motor via a solar powered Sepic converter-full bridge combination," *J. Power Electron.*, vol. 11, no. 5, pp. 743–750, Sep. 2011. [Online]. Available: https://jpels.org/digital-library/archives

[47] E. Hernández-Márquez, C. A. Avila-Rea, J. R. García-Sánchez, R. Silva-Ortigoza, M. Marciano-Melchor, M. Marcelino-Aranda, A. Roldán-Caballero, and C. Márquez-Sánchez, "'Full-bridge Buck inverter–DC motor' system: Steady-state and dynamic analysis and experimental validation," *Electronics*, vol. 8, no. 11, Nov. 2019, Art. no. 1216, doi: 10.3390/electronics8111216.

[48] R. Silva-Ortigoza, E. Hernández-Márquez, A. Roldán-Caballero, S. Tavera-Mosqueda, M. Marciano-Melchor, J. R. García-Sánchez, V. M. Hernández-Guzmán, and G. Silva-Ortigoza, "Sensorless tracking control for a 'full-bridge Buck inverter–DC motor' system: Passivity and flatness-based design," *IEEE Access*, vol. 9, pp. 132191–132204, 2021. [Online]. Available: https://ieeexplore.ieee.org/document/9536740

[49] R. Silva-Ortigoza, M. Marciano-Melchor, R. E. García-Chávez, A. Roldán-Caballero, V. M. Hernández-Guzmán, E. Hernández-Márquez, J. R. García-Sánchez, R. García-Cortés, and G. Silva-Ortigoza, "Robust flatness-based tracking control for a 'full-bridge Buck inverter–DC motor' system," *Mathematics*, vol. 10, no. 21, Nov. 2022, Art. no. 4110, doi: 10.3390/math10214110.

[50] V. M. Hernández-Guzmán, R. Silva-Ortigoza, and J. Orrante-Sakanassi, "Velocity control of a PMSM fed by an inverter-DC/DC Buck power electronic converter," *IEEE Access*, vol. 8, pp. 69448–69460, Apr. 2020. [Online]. Available: https://ieeexplore.ieee.org/document/9061159

[51] V. M. Hernández-Guzmán, "Velocity control of an induction motor fed by an inverter-DC/DC Buck power electronic converter," *Int. J. Control*, vol. 95, no. 7, pp. 1838–1849, Jul. 2022, doi: 10.1080/00207179.2021.1876925.

[52] V. M. Hernández-Guzmán, R. Silva-Ortigoza, S. Tavera-Mosqueda, M. Marcelino-Aranda, and M. Marciano-Melchor, "Path-tracking of a WMR fed by inverter-DC/DC Buck power electronic converter systems," *Sensors*, vol. 20, no. 22, Nov. 2020, Art. no. 6522, doi: 10.3390/s20226522.

[53] K. Lakomy, R. Madonski, B. Dai, J. Yang, P. Kicki, M. Ansari, and S. Li, "Active disturbance rejection control design with suppression of sensor noise effects in application to DC–DC Buck power converter," *IEEE Trans. Ind. Electron.*, vol. 69, no. 1, pp. 816–824, Jan. 2022, doi: 10.1109/TIE.2021.3055187.

[54] D. Izci, B. Hekimoğlu, and S. Ekinci, "A new artificial ecosystem-based optimization integrated with Nelder-Mead method for PID controller design of Buck converter," *Alex. Eng. J.*, vol. 61, no. 3, pp. 2030–2044, Mar. 2022, doi: 10.1016/j.aej.2021.07.037.

[55] O. Kaplan and F. Bodur, "Second-order sliding mode controller design of Buck converter with constant power load," *Int. J. Control*, vol. 96, no. 5, pp. 1210–1226, May 2023, doi: 10.1080/00207179.2022.2037718.

[56] M. A. Hassan, C.-L. Su, F.-Z. Chen, and K.-Y. Lo, "Adaptive passivity-based control of a DC–DC Boost power converter supplying constant power and constant voltage loads," *IEEE Trans. Ind. Electron.*, vol. 69, no. 6, pp. 6204–6214, Jun. 2022, doi: 10.1109/TIE.2021.3086723.

[57] R. S. Inomoto, J. R. B. A. Monteiro, and A. J. S. Filho, "Boost converter control of PV system using sliding mode control with integrative sliding surface," *IEEE J. Emerg. Sel. Topics Power Electron.*, vol. 10, no. 5, pp. 5522–5530, Oct. 2022, doi: 10.1109/JESTPE.2022.3158247.

[58] V. H. García-Rodríguez, J. H. Pérez-Cruz, R. C. Ambrosio-Lázaro, and S. Tavera-Mosqueda, "Analysis of DC/DC Boost converter–full-bridge Buck inverter system for AC generation," *Energies*, vol. 16, no. 6, Mar. 2023, Art. no. 2509, doi: 10.3390/en16062509.

[59] J. Linares-Flores, J. A. Juárez-Abad, A. Hernández-Méndez, O. Castro-Heredia, J. F. Guerrero-Castellanos, R. Heredia-Barba, and G. Curiel-Olivares, "Sliding mode control based on linear extended state observer for DC-to-DC Buck-Boost power converter system with mismatched disturbances," *IEEE Trans. Ind. Appl.*, vol. 58, no. 1, pp. 940–950, Jan. 2022, doi: 10.1109/TIA.2021.3130017.

[60] C.-Y. Chan, "Adaptive sliding-mode control of a novel Buck-Boost converter based on zeta converter," *IEEE Trans. Circuits Syst. II, Exp. Briefs*, vol. 69, no. 3, pp. 1307–1311, Mar. 2022, doi: 10.1109/TCSII.2021.3107315.

[61] M. Martinez-Lopez, J. Moreno-Valenzuela, and W. He, "A robust nonlinear PI-type controller for the DC–DC Buck-Boost power converter," *ISA Trans.*, vol. 129, pp. 687–700, Oct. 2022, doi: 10.1016/j.isatra.2022.01.016.

[62] D. Izci, S. Ekinci, H. L. Zeynelgil, and J. Hedley, "Performance evaluation of a novel improved slime mould algorithm for direct current motor and automatic voltage regulator systems," *Trans. Inst. Meas. Control*, vol. 44, no. 2, pp. 435–456, Jan. 2022, doi: 10.1177/01423312211037967.

[63] J. Wang, M. Li, W. Jiang, Y. Huang, and R. Lin, "A design of FPGA-based neural network PID controller for motion control system," *Sensors*, vol. 22, no. 3, Feb. 2022, Art. no. 889, doi: 10.3390/s22030889.

[64] X. Yang, W. Deng, and J. Yao, "Neural network based output feedback control for DC motors with asymptotic stability," *Mech. Syst. Signal Process.*, vol. 164, Feb. 2022, Art. no. 108288, doi: 10.1016/j.ymssp.2021.108288.

[65] Z. Gu, S. Yan, C. K. Ahn, D. Yue, and X. Xie, "Event-triggered dissipative tracking control of networked control systems with distributed communication delay," *IEEE Syst. J.*, vol. 16, no. 2, pp. 3320–3330, Jun. 2022, doi: 10.1109/JSYST.2021.3079460.

[66] V. M. Hernández-Guzmán, R. Silva-Ortigoza, and J. A. Orrante-Sakanassi, *Energy-Based Control of Electromechanical Systems: A Novel Passivity-Based Approach*. Cham, Switzerland: Springer, 2021.

[67] H. K. Khalil, *Nonlinear Systems*, 3rd ed. Upper Saddle River, NJ, USA: Prentice-Hall, 2002.

ROGELIO ERNESTO GARCÍA-CHÁVEZ received the B.S. degree in informatics engineering from Unidad Profesional Interdisciplinaria de Ingeniería y Ciencias Sociales y Administrativas (UPIICSA), Instituto Politécnico Nacional (IPN), Mexico City, Mexico, in 2022, and the M.S. degree in computing technology from CIDETEC-IPN, Mexico City, in 2023, where he is currently pursuing the Ph.D. degree with the Laboratory of Mechatronics and Renewable Energy.

His research interests include theory and application of automatic control in mechatronics systems, mobile robots, power electronics, and renewable energy.

RAMÓN SILVA-ORTIGOZA (Member, IEEE) received the B.S. degree in electronics from Benemérita Universidad Autónoma de Puebla (BUAP), Puebla, Mexico, in 1999, and the M.S. and Ph.D. degrees in electrical engineering, with a focus on mechatronics from Centro de Investigación y Estudios Avanzados del Instituto Politécnico Nacional (CINVESTAV-IPN), Mexico City, Mexico, in 2002 and 2006, respectively.

He has been a Researcher with the Department of Mechatronics and Renewable Energy, Centro de Innovación y Desarrollo Tecnológico en Cómputo, IPN (CIDETEC-IPN), since 2006, and belongs to SNII-CONAHCYT, Mexico. He has coauthored books, such as *Control Design Techniques in Power Electronics Devices* (Power Systems Series; London, U.K.: Springer-Verlag, 2006), *Automatic Control: Design Theory, Prototype Construction, Modeling, Identification and Experimental Tests* (Spanish; Mexico City, MX: CIDETEC-IPN, 2013), *Automatic Control with Experiments* (Advanced Textbooks in Control and Signal Processing Series; Cham, Switzerland: Springer Nature, 2019), and *Energy-Based Control of Electromechanical Systems: A Novel Passivity-Based Approach* (Advances in Industrial Control Series; Cham, Switzerland: Springer Nature, 2021). He has published over 80 articles in JCR indexed journals, 81 works in scientific divulgation journals and bulletins, and three chapters in international books. He has presented over 95 papers in conferences. He has been an advisor of over 35 postgraduate students and four B.S. students. Six of his students have been honored with the Presea Lázaro Cárdenas Award, in 2012, 2015, 2016, 2018, 2019, and 2020, the most important prize granted by IPN to its students, where also, three of these students, in 2015, 2017, and 2020, have also been honored with The Best Postgraduate Thesis Award. He has been the leader in more than 15 research projects and collaborated in 13 additional research projects. His research interests include mechatronic control systems, mobile robotics, control in power electronics, renewable energy, AC/DC motors, development of educational technology, and mathematical physics.

Dr. Silva-Ortigoza's research work has been cited over 3,000 times. He has been a reviewer in several JCR indexed journals. He has been a Referee in several awards of research and engineering, the National Program of Quality Postgraduate, and research projects of CONAHCYT. He was an Editor of the book *Mechatronics* (Spanish; Mexico City, MX: CIDETEC-IPN, 2010).

VICTOR MANUEL HERNÁNDEZ-GUZMÁN (Member, IEEE) was born in Querétaro, Mexico. He received the B.S. degree in electrical engineering from Instituto Tecnológico de Querétaro, Querétaro, in 1988, the M.S. degree in electrical engineering from Instituto Tecnológico de la Laguna, Torreón, Mexico, in 1991, and the Ph.D. degree in electrical engineering from CINVESTAV-IPN, Mexico City, Mexico, in 2003.

He has been a Professor with Universidad Autónoma de Querétaro, Querétaro, since 1995, where he teaches classical and nonlinear control. He has coauthored books, such as *Automatic Control: Design Theory, Prototype Construction, Modeling, Identification and Experimental Tests* (Spanish; Mexico City, MX: CIDETEC-IPN, 2013), *Automatic Control with Experiments* (Advanced Textbooks in Control and Signal Processing Series; Cham, Switzerland: Springer Nature, 2019), and *Energy-Based Control of Electromechanical Systems: A Novel Passivity-Based Approach* (Advances in Industrial Control Series; Cham, Switzerland: Springer Nature, 2021). He has published over 45 articles in refereed journals. His research interests include control of mechatronic systems, mobile robots, and electromechanical systems. This includes control of different classes of AC electric motors when actuating on complex nonlinear mechanical loads. His research interests include prototype construction to teach classical and nonlinear control techniques.

MAGDALENA MARCIANO-MELCHOR received the B.S., M.S., and Ph.D. degrees in mathematics from Benemérita Universidad Autónoma de Puebla, Puebla, Mexico, in 1999, 2002, and 2006, respectively.

She has been a Professor and a Researcher with CIDETEC-IPN, since 2007. She has been an advisor of several postgraduate students. She has been the Leader of research projects with IPN. She belongs to SNII-CONAHCYT, Mexico, and the Mexican Societies of Physics and Mathematics. She has published several papers in JCR indexed journals. Her research interests include dynamic systems, control theory, and mathematical physics.

ÁNGEL ADRIÁN ORTA-QUINTANA received the B.S. degree in control and automation engineering from Escuela Superior de Ingeniería Mecánica y Eléctrica, Instituto Politécnico Nacional (ESIME-IPN), Mexico City, Mexico, in 2022. He is currently pursuing the M.S. degree with the Department of Mechatronics and Renewable Energy, CIDETEC-IPN.

His research interest includes the control application of control systems in industrial processes and their instrumentation.

JOSÉ RAFAEL GARCÍA-SÁNCHEZ received the B.S. degree in industrial robotics from ESIME-IPN, Mexico City, Mexico, in 2003, the M.S. degree in automatic control from Universidad Nacional Autónoma de México, Mexico City, in 2013, and the Ph.D. degree in engineering of robotic and mechatronic systems from CIDETEC-IPN, Mexico City, in 2018.

He is currently a Professor and a Researcher with the Department of Mechatronics, Tecnológico de Estudios Superiores de Huixquilucan, Tecnológico Nacional de México, and belongs to SNII-CONAHCYT, Mexico. He has published and presented papers in JCR indexed journals and international conferences, respectively. His research interests include the theory and application of automatic control in mobile robotics, teleoperated systems, and power electronic systems. During his academic trajectory, he was a recipient of the Distinction to Polytechnic Merit: Presea Lázaro Cárdenas 2018, in the physical and mathematical sciences area at Ph.D. level.

HIND TAUD (Member, IEEE) received the B.S. degree in physical sciences from Université Sidi Mohamed Ben Abdellah, Fez, Morocco, the M.S. and Ph.D. degrees in physical sciences from Université Mohammed V, Rabat, Morocco, and the Ph.D. degree in earth science from Université Paris VI, Paris, France.

She was an AUPELF-UREF Postdoctoral Fellow with Université Paris VI. She was with Universidad Nacional Autónoma de México, before joining Instituto Mexicano del Petróleo. She is currently with Instituto Politécnico Nacional, Mexico City, Mexico. Her research interests include electronics, geospatial information analysis, computer vision, pattern recognition, machine learning, and deep learning.